Environmental Science & Technology

pubs.acs.org/est

Article

Underestimated Sink of Atmospheric Mercury in a Deglaciated Forest Chronosequence

Xun Wang,* Wei Yuan, Che-Jen Lin, Ji Luo, Feiyue Wang, Xinbin Feng,* Xuewu Fu, and Chen Liu

Cite This: *Environ. Sci. Technol.* 2020, 54, 8083−8093

Read Online

ACCESS | Metrics & More | Article Recommendations | Supporting Information

ABSTRACT: Mercury (Hg) deposition through litterfall has been regarded as the main input of gaseous elemental mercury (Hg^0) into forest ecosystems. We hypothesize that earlier studies largely underestimated this sink because the contribution of Hg^0 uptake by moss and the downward transport to wood and throughfall is overlooked. To test the hypothesis, we investigated the Hg fluxes contributed via litterfall and throughfall, Hg pool sizes in moss covers and woody biomass as well as their isotopic signatures in a glacier-to-forest succession ecosystem of the Southeast Tibetan Plateau. Results show that Hg^0 depositional uptake and pool sizes stored in moss and woody biomass increase rapidly with the time after glacier retreat. Using the flux data as input to a Hg isotopic mixing model, Hg deposition through litterfall accounts for 27−85% of the total accumulation rate of Hg^0 in organic soils of glacial retreat over 20−90 years, revealing the presence of additional sources of Hg^0 input. Atmospheric Hg^0 accounts for 76 ± 24% in ground moss, 86 ± 15% in tree moss, 62−92% in above ground woody biomass (branch−bark−stem), and 44−83% in roots. The downward decreasing gradient of atmospheric Hg^0 fractions from the above ground woody biomass to roots suggests a foliage-to-root Hg transport in vegetation after uptake. Additionally, 34−82% of atmospheric Hg^0 in throughfall further amplifies the accumulation of Hg^0 from atmospheric sources. We conclude that woody biomass, moss, and throughfall represent important Hg^0 sinks in forest ecosystems. These previously unaccounted for sink terms significantly increase the previously estimated atmospheric Hg^0 sink via litterfall.

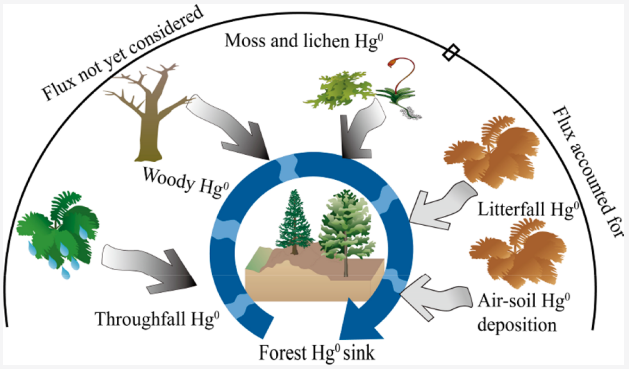

1. INTRODUCTION

Anthropogenic mercury (Hg) emissions during the past ∼150 years have increased the present atmospheric Hg deposition quantity by 3−5 times of that during the preindustrial period and have resulted in elevated Hg levels in even the most remote ecosystems.[1−5] Forest ecosystems are important receptors of atmospheric Hg and sources of Hg in aquatic systems.[6,7] Hg deposition in forest ecosystems comes from precipitation or throughfall, and Hg^0 uptake increases by vegetation and soil.[7,8] Throughfall Hg accounts for most wet and Hg^{2+} dry deposition, while litterfall Hg accounts for mainly Hg^0 dry deposition.[9,10] Global Hg deposition through litterfall is estimated to be ∼1200 Mg yr^{-1}, equivalent to 50−60% of total annual anthropogenic Hg emissions.[10]

The knowledge of the Hg biogeochemical cycle in forests has been greatly improved through recent investigations on Hg isotope compositions of forest ecosystems.[11,12] Hg mass-dependent fractionation (MDF, reported as δ^{202}Hg) and mass-independent fractionation (MIF, reported as Δ^{199}Hg, Δ^{200}Hg, and Δ^{201}Hg) can be employed to trace sources of Hg deposition and identify processes responsible for Hg transformation and retention in forest ecosystems. Earlier flux measurements suggest that Hg in alpine forest ecosystems is mainly from Hg^{2+} wet positions via precipitation, throughfall, and cloudwater,[13−15] but recent evidence from Hg stable isotope analysis supports dry deposition of Hg^0 as being the primary source.[16−20] This discrepancy represents a significant knowledge gap in Hg cycling across the atmosphere−vegetation−soil interface. We hypothesize that many previous flux measurement studies in forest ecosystems have underestimated the atmospheric Hg^0 sink because they ignored the role of moss and lichen in taking up atmospheric Hg^0, Hg^0 contribution in throughfall, as well as the Hg^0 mass stored in woody biomass caused by Hg translocation after deposition.

Hg widely distributed in forest trees and on the forest ground, moss, and lichen contributes to 15−20% of total net primary production in boreal and temperate forests.[21] High Hg concentrations have been measured in moss and lichen,[22−24] which are primarily of atmospheric origin.[18,25,26] While earlier studies have generally focused on the use of moss and lichen as

Received: March 17, 2020
Revised: June 6, 2020
Accepted: June 8, 2020
Published: June 8, 2020

https://dx.doi.org/10.1021/acs.est.0c01667
Environ. Sci. Technol. 2020, 54, 8083−8093

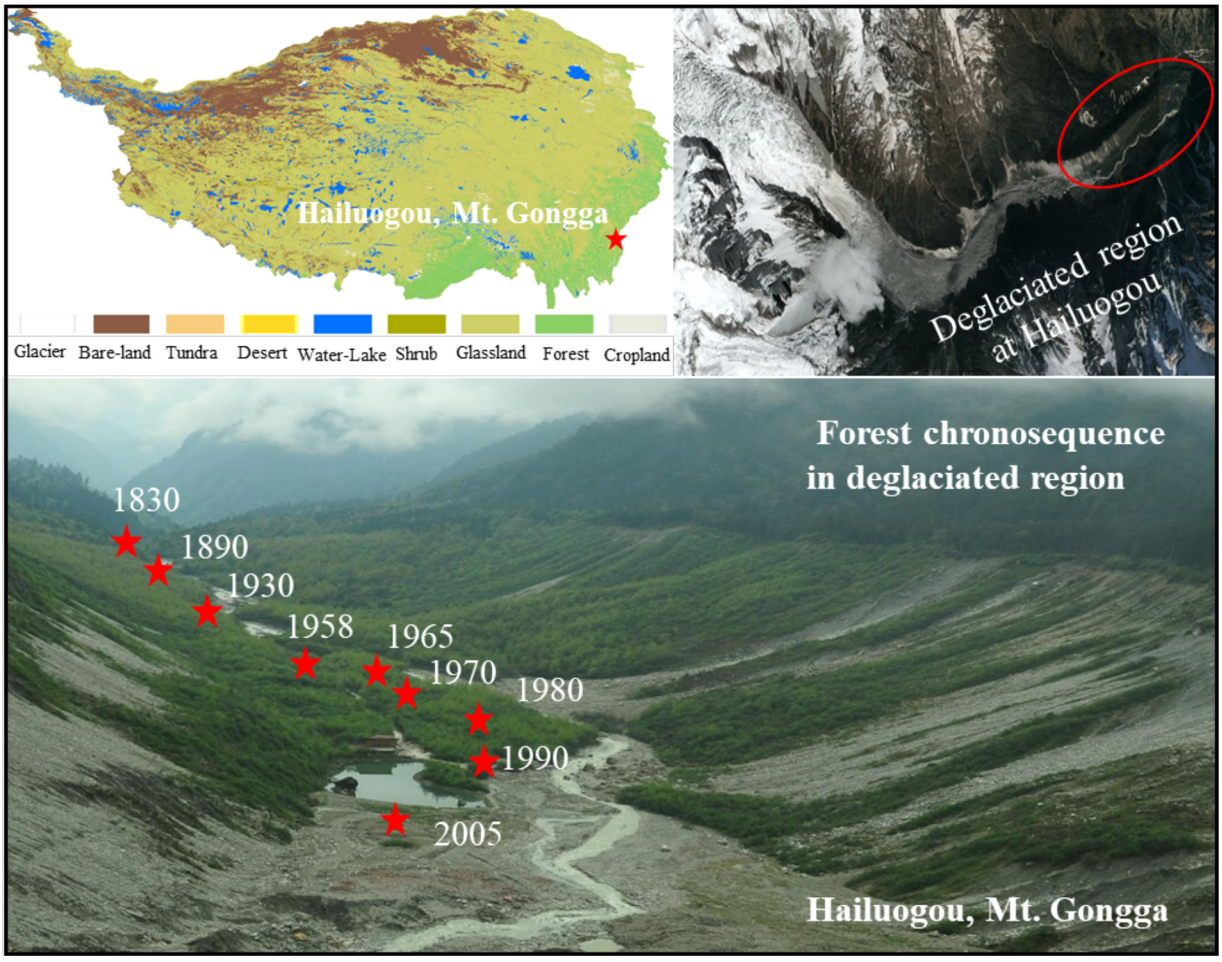

Figure 1. Sampling sites in a forest chronosequence at the deglaciated terrain of Hailuogou, Mt. Gongga in the Southeast Tibetan Plateau, China. The site representing the 2005 glacier retreat is inhabited by small pioneer tree species including big leaf poplars (*Populus purdomii* Rehd.), common sea buckthorns (*Hippophae rhamnoides* Linn.), and willows (*Salix magnifica* Hemsl.). At the sites representing the 1958 retreat, poplars become the dominant species, and at the sites representing the retreats in 1890−1958, poplars are gradually replaced by the Faber's firs (*Abies fabri* (Mast.) Craib) and dragon spruces (*Picea asperata* Mast.). The dendroglaciology of glacier retreated time has been determined previously in detail by our earlier studies.[38,39] The land use of the Tibet Plateau in 2015 is from the National Tibetan Plateau Data Center, China.

bioindicators to monitor the Hg pollution levels,[27−29] few studies have assessed the contribution of moss and lichen to atmospheric Hg^0 deposition in forest ecosystems. In addition, Hg deposition from precipitation and litterfall shows distinct Hg isotopic compositions, especially in their MIF signatures,[16,20,30,31] while the Hg isotopic signatures in throughfall are unknown. Hg in throughfall is suggested to originate from particulate-bounded Hg (PBM) and gaseous oxidized Hg (GOM) that are washed off from leaf surfaces during rainfall events.[32−34] Photoreduction of PBM and GOM at the surface of foliage[17,20] and their mixing with detritus of biomass (e.g., bark, lichen, moss) may shift the Hg MIF signals in throughfall.[35] In addition, Hg in above ground woody biomass can exceed Hg stored in foliage by 1−2 times.[11,36] Atmospheric Hg^0 has been suggested as the main source in woody biomass under artificial laboratory conditions,[37] yet the quantity of Hg stored in woody biomass as a sink is unknown.

In this study, we show the results of a comprehensive study at a forest chronosequence site in the Southeast Tibetan Plateau (TP) region to test the hypothesis that atmospheric Hg^0 sink is significantly underestimated because the contribution of Hg^0 uptake by moss and the downward transport to wood and throughfall is overlooked. We choose to use this forest chronosequence site since glacier-to-vegetation succession changes the landscape and provides a unique opportunity to study the sources and accumulation of Hg over time in terrestrial ecosystems. After glacial retreat, the deglaciated region continuously receives atmospheric deposition, allowing for the ability to study the fate of deposited Hg and subsequent transport and accumulation across the air−soil−plant−water interface of the forest ecosystems over a time period of hundreds of years. Our earlier studies suggest that the recession of glaciers is followed by rapid establishment of vegetative ecosystems that capture 2−3 times more atmospheric Hg than the Hg released from glacier melting.[25,38] Combining the input of Hg to forest soil in our earlier research,[38] this study presents new data of Hg isotopic signatures in the samples of moss and lichen covers grown on ground and vegetation, in woody biomass, and in throughfall to infer their Hg sources and accumulation processes in the whole forest chronosequence ecosystems. Implications of this atmospheric Hg^0 deposition term on the global Hg cycling are also discussed.

https://dx.doi.org/10.1021/acs.est.0c01667
Environ. Sci. Technol. 2020, 54, 8083−8093

2. METHODS

2.1. Site Descriptions. The Hailuogou Glacier, located in the Southeast TP, is one of the major glacier systems on the east slope of Mt. Gongga (101°30′∼102°15′ E, 29°20′∼30°20′ N; peak elevation: 7556 m above sea level, Figure 1). The glacier has been retreating since the Little Ice Age (∼1830) due to the global warming. The glacier retreat area at the elevation of 2950−3000 m has a complete primary forest chronosequence over a distance of ∼2 km. A glacier retreat period of 1830−2005 has been determined previously as described in our earlier work[38,39] and in the Supporting Information (SI, Section S1). Briefly, the big leaf poplar (*Populus purdomii* Rehd.), common sea buckthorn (*Hippophae rhamnoides* Linn.), and willow (*Salix magnifica* Hemsl.) are the dominant tree species at the site representing the most recent glacier retreat during 2005. At the sites of retreat during 1958, poplars become the dominant species and then are gradually replaced by the Faber's fir (*Abies fabri* (Mast.) Craib) and dragon spruce (*Picea asperata* Mast.) at sites of glacier retreat in 1958−1890.

2.2. Sampling. The protocols for sampling the vegetation biomass, precipitation, and throughfall have been described in detail elsewhere[38,39] and in Sections S1 and S2 of the Supporting Information. Briefly, eight sites were selected for vegetation sampling on the basis of the glacier retreat time (2005, 1990, 1980, 1970, 1958, 1930, 1890, and 1830), and seven sites (1990, 1980, 1970, 1965, 1958, 1930, and 1890) were selected for moss and lichen growth on the ground and canopy and litterfall deposition sampling. The collection of open precipitation (glacier retreat time: 2005) and throughfall (seven sites at glacier retreat times: 1990, 1980, 1970, 1965, 1958, 1930, and 1890) was made during September 2017−September 2019.

The collection of all vegetation samples at eight sampling sites was conducted in September−October of 2017. For the woody biomass sampling, each tree was separated into foliage, branches, stems, barks, and roots including fine (diameter <2 mm), medium (2−30 mm), and coarse (>30 mm) ones. While lichen cover was observed on only a few scattered tree stems, an intensive moss cover was widespread on the trees and ground. Due to its overwhelming biomass, this study mainly focuses on the role of moss cover. The detailed methodology for moss covers and monthly litterfall sampling is in Section S1 of the Supporting Information.

2.3. Concentration and Stable Hg Isotopic Measurements. Mercury concentrations of the vegetation and litterfall samples were measured on a DMA80 Hg analyzer,[16,40] and the total Hg concentrations in water samples were determined following US EPA Method 1631 using a Tekran 2500 as the Hg detector.[41] More details can be found in Section S3 of the Supporting Information. Specific Hg pool sizes and litterfall deposition were estimated for each site on the basis of the measured Hg concentration and the biomass production. The annual Hg depositions through precipitation and throughfall were estimated by the Hg concentration and rainfall or throughfall amount.

The Hg concentration in the same tree species is comparable at different deglaciated sites (Figure S1). Thus, we chose the big leaf poplar, common sea buckthorn, and willow grown at the site of 1958 and Faber's fir and dragon spruce grown at the site of 1930 to measure the Hg isotopic signatures. Precipitation and throughfall samples collected during September−November 2017 were analyzed by the Hg isotopic signatures, following the method described by Li et al.[42] More details can be found in Section S4 of the Supporting Information. Briefly, 5 L of water (about 10−35 ng Hg) was collected by a precipitation collector and filtered through cellulose membranes with 0.45 μm pore size. Variable volumes (5−20 mL) of BrCl (depending on the DOC content in water[42]) and 200 μL of $SnCl_2$ were successively added into the water samples to purge and trap the generated Hg^0 into a chlorinate carbon trap (CCT, 1 g weight). This approach of adding BrCl alone in filtered water released 96 ± 5% of Hg from the water samples (Table S1).

The procedure for Hg isotope measurement of vegetation, cellulose membranes, and CCT samples has been described previously[16,42] and can be found in Section S5 of the Supporting Information. Briefly, all samples were processed by a double-stage tube furnace and trapping solutions (anti aqua regia, HNO_3/HCl = 2:1, v/v) for Hg preconcentration. The preconcentrated Hg solutions were diluted to 1 ng mL^{-1} prior to Hg isotope measurement on a Nu-Plasma II multicollector-inductively coupled plasma mass spectrometer (MC-ICP-MS). The cellulose membranes and CCT samples from the same throughfall samples were mixed to obtain the Hg isotopic signatures of bulk throughfall. The recoveries of preconcentration ranged from 95 to 103% for the standard reference materials (lichen standard reference, BCR-482 from the European Commission) and from 91 to 105% for all samples (Table S1−S3). Concentrations and acid matrices of Hg standard solutions (NIST-3133 and the UM-Almadén secondary standard solution) were matched to the sample solutions. Hg-MDF is reported in the δ notation referenced to the neighboring NIST-3133 solution:

$$\delta^{202}\mathrm{Hg}\ (‰) = 1000 \times [(^{202}\mathrm{Hg}/^{198}\mathrm{Hg}_{\mathrm{sample}}) / (^{202}\mathrm{Hg}/^{198}\mathrm{Hg}_{\mathrm{NISTSRM3133}}) - 1] \quad (1)$$

MIF is reported as Δ^{xxx}Hg following the convention suggested by Blum and Bergquist:[43]

$$\Delta^{199}\mathrm{Hg}\ (‰) = \delta^{199}\mathrm{Hg} - 0.2520 \times \delta^{202}\mathrm{Hg} \quad (2)$$

$$\Delta^{200}\mathrm{Hg}\ (‰) = \delta^{200}\mathrm{Hg} - 0.5024 \times \delta^{202}\mathrm{Hg} \quad (3)$$

$$\Delta^{201}\mathrm{Hg}\ (‰) = \delta^{201}\mathrm{Hg} - 0.7520 \times \delta^{202}\mathrm{Hg} \quad (4)$$

The UM-Almadén secondary standard was analyzed for every 10 samples. Results of UM-Almadén (δ^{202}Hg = −0.53 ± 0.04‰, Δ^{199}Hg = −0.00 ± 0.04‰, Δ^{201}Hg = −0.03 ± 0.02‰, mean ±1 standard deviation, n = 59) and BCR-482 (δ^{202}Hg = −1.65 ± 0.08‰, Δ^{199}Hg = −0.56 ± 0.04‰, Δ^{201}Hg = −0.58 ± 0.04‰, n = 12) were consistent with the recommended values.[43,44]

2.4. Modeling. A triple endmember mixing model by two-dimensional Hg MIF signatures[16−20] was constructed for tracing Hg sources in woody biomass:

$$F_1 + F_2 + F_3 = 1 \quad (5)$$

$$F_1 \times \Delta^{199}\mathrm{Hg}_1 + F_2 \times \Delta^{199}\mathrm{Hg}_2 + F_3 \times \Delta^{199}\mathrm{Hg}_3 = \Delta^{199}\mathrm{Hg}_{\mathrm{wood}} \quad (6)$$

https://dx.doi.org/10.1021/acs.est.0c01667
Environ. Sci. Technol. 2020, 54, 8083−8093

$$F_1 \times \Delta^{200}Hg_1 + F_2 \times \Delta^{200}Hg_2 + F_3 \times \Delta^{200}Hg_3 = \Delta^{200}Hg_{wood} \quad (7)$$

where F_i is the fraction ratio of endmember i (i = 1, 2, 3, denoting the atmospheric Hg^0 input, atmospheric Hg^{2+} input, and geological source, respectively). Our earlier studies[25,38] have documented that the mean Hg MIF signatures obtained from rock and soil under 5 cm of the C horizon (Δ^{199}Hg, 0.16 ± 0.07‰ and Δ^{200}Hg, 0.01 ± 0.04‰) can be used as the signatures of geological input endmember, the Hg MIF signatures in precipitation (Δ^{199}Hg, 0.91 ± 0.27‰ and Δ^{200}Hg, 0.19 ± 0.04‰) can be used to represent atmospheric Hg^{2+} input endmember, and the MIF signatures of foliage (Δ^{199}Hg, −0.23 ± 0.05‰ and Δ^{200}Hg, −0.04 ± 0.04‰) can be used to represent atmospheric Hg^0 input endmember.

A two-endmember mixing model with Δ^{199}Hg signatures (eqs 8 and 9) and Δ^{200}Hg signatures (eqs 10 and 11) of atmospheric Hg^0 and Hg^{2+} inputs was applied to estimate the contribution of Hg sources in moss and in throughfall:

$$F_{41} + F_{51} = 1 \quad (8)$$

$$F_{41} \times \Delta^{199}Hg_4 + F_{51} \times \Delta^{199}Hg_5 = \Delta^{199}Hg_{moss\ or\ throughfall} \quad (9)$$

$$F_{42} + F_{52} = 1 \quad (10)$$

$$F_{42} \times \Delta^{200}Hg_4 + F_{52} \times \Delta^{200}Hg_5 = \Delta^{200}Hg_{moss\ or\ throughfall} \quad (11)$$

where F_i is the fraction ratio of endmember i (i = 4, 5, denoting the atmospheric Hg^0 input and atmospheric Hg^{2+} input). F_{41} and F_{51} are estimated from the Δ^{199}Hg-mixing model, and F_{42} and F_{52} are estimated from the Δ^{200}Hg-mixing model. A Monte Carlo simulation was applied to generate one million groups of MIF signatures, which randomly range from one standard deviation (SD) below the mean to one SD above the mean. Finally, the fraction ratio was estimated as the average of these solutions, which ranges from 0 to 1, during one million times of solving eqs 5−11. The two estimation methods (based on Δ^{200}Hg, eqs 8 and 9 and Δ^{199}Hg, eqs 10 and 11) yielded reasonable agreement with each other (Table S4). Given that there are uncertainties of the Hg isotopic mixing models (discussed in detail in Section 4.6), they do not follow one another exactly. To better estimate the source, we averaged the two methods as

$$F_4 = (F_{41} + F_{42})/2 \quad (12)$$

$$F_5 = (F_{51} + F_{52})/2 \quad (13)$$

2.5. Statistical Analysis. The Hg isotopic mixing models and Monte Carlo simulations were conducted using MATLAB. ANOVA test and paired t test for data were performed by SPSS 20.0. We applied a two-level factorial design of experiments using Minitab 6.0 to analyze the model sensitivity caused by the changes in Hg isotopic signatures of endmembers. The factorial design of the experiments is meant to gauge the extreme variation caused by the possible range of model parameters. In short, Hg MIF values from each endmember were varied individually and in combinations at the two selected levels (i.e., a high value and a low value). The high level is set as the mean + 2SD for the Hg MIF value in each endmember, and the low level is set as the mean − 2SD.

3. RESULTS

3.1. Variation in Hg Deposition Fluxes and Pools during Forest Succession. Leaf litter Hg deposition ranges from 7.7−14.8 μg m^{-2} yr^{-1} during the first 20−60 years after glacier retreat (1990−1958 retreat sites) and 31.0−43.1 μg m^{-2} yr^{-1} beyond 90 years after glacier retreat (1930−1890 retreat sites, Figure 2a). Twig litter Hg deposition ranges from

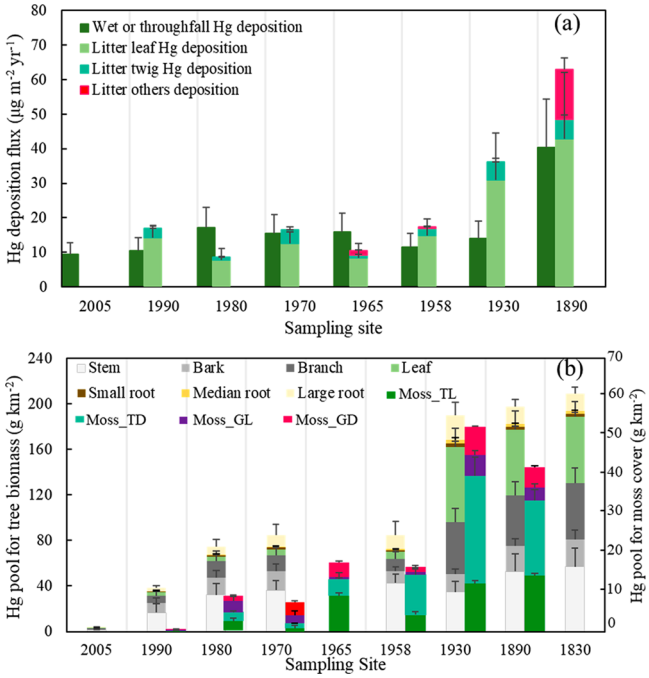

Figure 2. (a) Atmospheric Hg deposition via litterfall, precipitation (the site of 2005 retreat), throughfall, and the litter others that mainly include the detritus of bark, lichen, moss, etc.. (b) Variation of Hg pool size in the main components of tree species and in moss grown on trees and on ground in the forest chronosequence zone, Mt Gongga. TL is the moss live foliage on the tree, TD is the moss dead parts on the tree, GL is the moss live foliage on the ground, and GD is the moss dead parts on the ground.

0.8−3.8 μg m^{-2} yr^{-1} at the sites of 1958−1990 retreat and increases to 5.2−5.6 μg m^{-2} yr^{-1} at the sites of 1890−1990 retreat. Deposition fluxes observed for tree detritus (e.g., bark, lichen, moss) show a significant difference at the sites of the 1958−1965 retreat, especially at the site of the 1890 retreat (up to 14.6 μg m^{-2} yr^{-1}). The rapid increase in Hg deposition via litterfall at the older sites (i.e., 1890−1930 retreat sites) is caused by the higher Hg concentration (78−97 versus 33−41 ng g^{-1}, Table S5) and greater litter biomass production (398−444 versus 212−443 g m^{-2}, Table S5) in the coniferous litter compared to the deciduous litter.

Annual Hg deposition through open precipitation (site of the 2005 retreat) is 9.4 ± 3.5 μg m^{-2} yr^{-1} (Figure 2a). Although the throughfall Hg concentration is 1−2 times as the Hg concentration in precipitation in the open area, water retention by canopy leads to the smaller throughfall depth (Table S5) at sites of the 1930−1990 retreat. Thus, the throughfall Hg depositions at these sites are comparable to the flux of open field wet Hg deposition. The higher throughfall Hg deposition at the site representing the 1890 retreat is caused by the unusually elevated throughfall Hg concentration (about 6 times higher than in precipitation, Table S5). The

https://dx.doi.org/10.1021/acs.est.0c01667
Environ. Sci. Technol. 2020, 54, 8083−8093

litterfall Hg deposition flux is comparable to the throughfall Hg deposition flux at most sites, except for the 1930 site where litterfall Hg deposition flux is 2 times as the throughfall Hg deposition flux (Figure 2a).

The total Hg pool size in tree components increases with the glacier retreated time, ranging from 3.9 g km^{-2} at the site representing the glacial retreat time of 2005 to 228.8 g km^{-2} at the site of 1830 (Figure 2b). Three stages of evolution for Hg pool size in tree components (Figure 2b and Table S6) can be distinguished during forest succession. Foliage Hg accounts for 32 ± 10% of total pool size in the most recent succession period (~10 years after glacier retreat, i.e., 2005 site), drops to only 7−11% as the forest matures (20−60 years after glacier retreat, i.e., 1990−1958 sites), and then recovers to 30−35% at sites with the earliest retreat (~90 years after glacier retreat, i.e., 1930 retreat site).

Figure 2b depicts the variation of Hg pool size in moss grown on ground and trees. The Hg pool size in live moss foliage on the tree is comparable to the pool size on the ground across the sites of 1990−1970 retreat, both ranging from 0.8 to 2.9 g km^{-2}, but is 2−10 times smaller than the size in live moss foliage on the trees at sites of 1965−1890 retreat because of the higher stem surface area of these older trees. The coniferous site has a denser moss cover, leading to up to 3.3−5.4 g km^{-2} pool size in live moss foliage on ground and 12.2−14.1 g km^{-2} pool size on the trees. The sum of Hg pool size in live moss foliage on ground and canopy ranges from 1.8 to 9.7 g km^{-2} at the sites of 1958−1990 retreat, comparable to the Hg pool size in tree foliage (1.0−5.8 g km^{-2}, p = 0.548 by paired t test). The total Hg pool size in live moss foliage is 17.3−17.6 g km^{-2} at sites of 1890−1930 retreat, which is 3−4 times lower than that in tree foliage (Figure 2b). The Hg pool size in dead moss biomasses (i.e., root and dead moss foliage) either on the ground or canopy is 1−3 times larger than in the live moss foliage (Figure 2b).

3.2. Mercury Isotopic Compositions. Parts a and b of Figure 3 depict Hg isotopic signatures in the tree woody biomass. The MDF signatures (δ^{202}Hg) in woody biomass vary among the tree species and tree components. Coniferous tree species have more negative δ^{202}Hg values than deciduous tree species (−3.15 ± 0.22‰ versus −2.39 ± 0.51‰, Table S2). The average values of δ^{202}Hg in tree biomass samples are −3.16 ± 0.46‰ for bark, −2.80 ± 0.49‰ for stem, −2.64 ± 0.74‰ for branch, −2.76 ± 0.29‰ for large root, −2.63 ± 0.39‰ for medium root, and −2.43 ± 0.35‰ for small root (Table S2). Only the δ^{202}Hg in bark is significantly higher than in small root (p < 0.05 by ANOVA test). The average values of Δ^{199}Hg show an increasing trend from branch (−0.16 ± 0.04‰), bark (−0.16 ± 0.11‰), stem (−0.14 ± 0.05‰), large root (−0.04 ± 0.11‰), small root (0.00 ± 0.10‰) to medium root (0.03 ± 0.11‰). Tree species have little influence on the Δ^{199}Hg variation. The Δ^{200}Hg values are nearly 0 in all woody biomass samples.

The Hg isotopic signatures in the moss or lichen samples are comparable at different deglaciated sites (Table S3). All values of Δ^{200}Hg in moss and lichen are close to 0. Tree lichen has a more negative δ^{202}Hg value (−3.50 ± 0.27‰ for lichen versus −2.64 ± 0.24‰ for moss) and a more positive Δ^{199}Hg value than those in tree moss (−0.07 ± 0.04‰ for lichen versus −0.21 ± 0.04‰ for moss). The ground moss has more positive δ^{202}Hg, Δ^{199}Hg, and Δ^{200}Hg values than the tree moss (δ^{202}Hg, Δ^{199}Hg, and Δ^{200}Hg: −2.05 ± 0.12, −0.03 ± 0.07, and 0.01 ± 0.04‰ for ground moss versus −2.64 ± 0.24, −0.21 ± 0.04, and −0.02 ± 0.04‰ for tree moss).

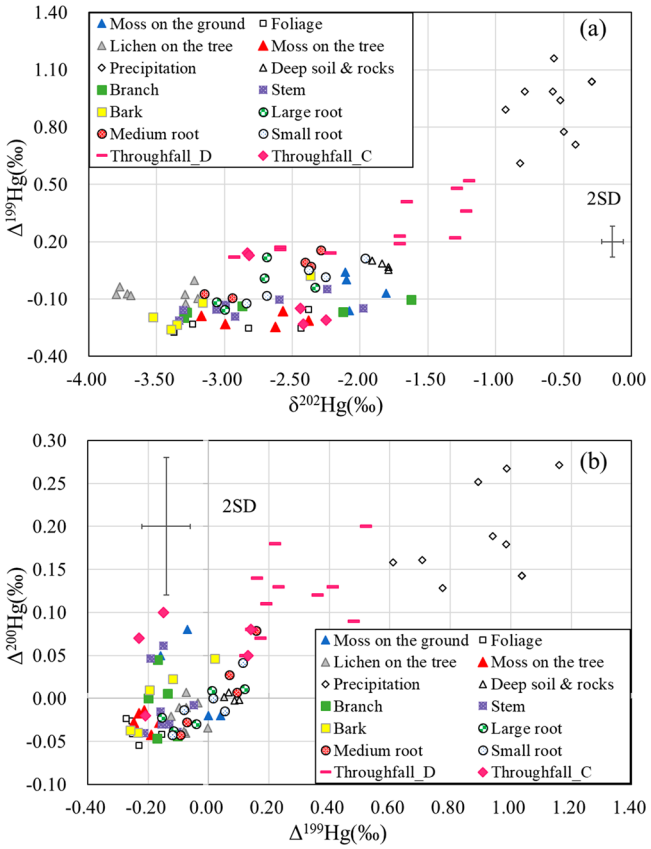

Figure 3. Hg isotopic signatures in (a and b) precipitation, woody biomass, deep soil and rocks, lichen, moss on trees and on ground, throughfall of deciduous forest ("Throughfall_D", at the 1990, 1980, 1970, and 1958 retreat sites), and throughfall of coniferous forests ("Throughfall_C", at the 1930, 1890, and 1830 retreat sites). The Hg isotopic signatures of precipitation, deep soil, and rocks have been documented in our earlier study.[38]

Both MIF and MDF signatures of Hg in throughfall observed in this study are significantly more negative than those in precipitation (p < 0.001, Figure 3a,b). The Hg isotopic signatures in throughfall at the 1990 retreat site (δ^{202}Hg, Δ^{199}Hg, and Δ^{200}Hg: −1.25 ± 0.07, 0.37 ± 0.21, and 0.18 ± 0.04‰) are close to the signatures of precipitation but gradually shift to the signatures of endmember for the vegetation covers (e.g., bark, foliage, moss, and lichen on canopy) at the 1890 site (δ^{202}Hg, Δ^{199}Hg, and Δ^{200}Hg: −2.37 ± 0.10, −0.19 ± 0.04, and 0.05 ± 0.04‰). Specifically, both Δ^{199}Hg and Δ^{200}Hg show significant negative correlations with the throughfall flux (r = −0.89, p < 0.001 for Δ^{199}Hg and r = −0.53, p < 0.05 for Δ^{200}Hg).

4. DISCUSSION

4.1. Transitions of Hg Pools in Tree Components during Deglaciated Forest Chronosequence. Three stages of evolution for Hg pool size cannot be explained by the variation of Hg concentrations in woody biomass (branch−stem−bark−root) since the values are similar among tree species (Figure S1, p = 0.053−0.869, ANOVA test). The evolution in Hg pool distribution in tree components is most likely caused by the vegetative development at different stages of forest succession because of their

https://dx.doi.org/10.1021/acs.est.0c01667
Environ. Sci. Technol. 2020, 54, 8083−8093

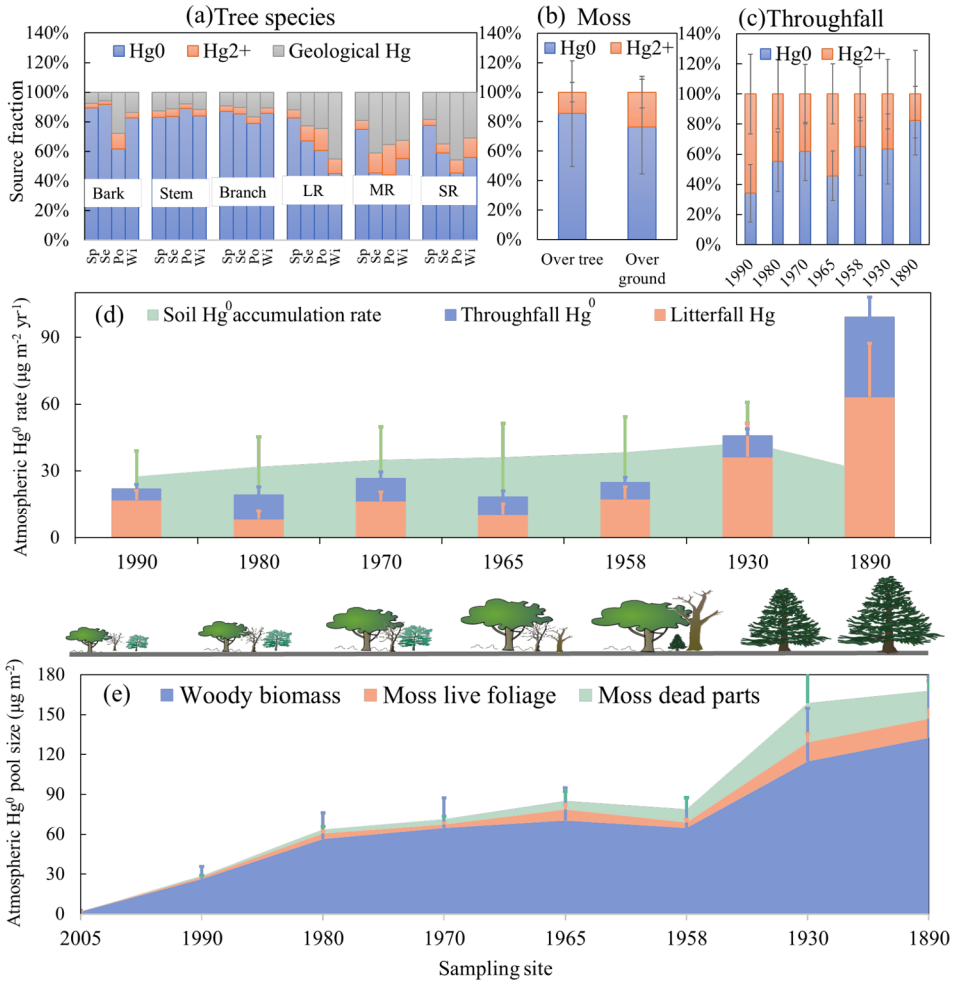

Figure 4. (a) Atmospheric Hg^0, atmospheric Hg^{2+}, and geological Hg source fractions in woody biomass (Sp, spruce; Se, common sea buckthorn; Po, big leaf poplar; Wi, willow; LR, large root (>30 mm); MR, medium root (2−30 mm), and SR, small root <2 mm). (b) Atmospheric Hg^0 and Hg^{2+} source fractions in moss on trees and on the ground. (c) Atmospheric Hg^0 and Hg^{2+} source fractions in throughfall. (d) Variations of atmospheric Hg^0 deposition fluxes in throughfall and in litterfall, and atmospheric Hg^0 accumulation rate in organic soils. (e) Variations of atmospheric Hg^0 pool size in total moss covers and in woody biomass. The atmospheric Hg^0 accumulation rate in organic soils is derived from our earlier study.[38] The uncertainties in Hg source fractions in woody biomass are as following: 25% for atmospheric Hg^0, 9% for atmospheric Hg^{2+}, and 14% for geological Hg.

competitive strategies, with tree species with a greater woody mass competing more favorably during forest succession.[45] The woody biomass increases 49 times from the site of 2005−1958 retreat, while foliage biomass increases 4 times; woody biomass increases 1.5 times from the site of 1958−1830 retreat, while foliage biomass increases 6 times (Table S7).

4.2. Hg Sources in Woody Biomass. The more negative δ^{202}Hg value in coniferous woody components than in deciduous woody components agrees with other studies[17,20,38] reporting much lighter ^{202}Hg values in coniferous tree species. The differences in δ^{202}Hg between deciduous and coniferous trees are likely due to the colocated species-specific differences in ^{202}Hg fractionation during foliar uptake.[46] The increasing δ^{202}Hg from above ground biomasses to roots can be attributed two reasons. One is that the higher contribution from geological Hg and atmospheric Hg^{2+} sources (more positive δ^{202}Hg value than in foliage) in root. The other is the possible ^{202}Hg fractionation during Hg transport among wood components. However, little direct evidence can support this hypothesis, and we recommend more studies on this issue.

The processes causing ^{199}Hg MIF, which include magnetic isotope effect (MIE) and nuclear volume effect (NVE), do not occur during the Hg transport among the tree deferment components.[46] Hence, the distinct increase of Δ^{199}Hg value from branch to root indicates a different Hg source mixing ratio. Results from the triple endmember mixing model (Figure 4a) show that atmospheric Hg^0 is the dominant source in the above ground woody biomass (branch−bark−stem). Atmospheric Hg^0 accounts for 79−87% (mean = 84 ± 25%, 1SD based on the uncertainty of Hg isotopic mixing model) of Hg in branch, 62−92% (mean = 81 ± 25%) in bark, and 83−88% (mean = 84 ± 25%) in stem. Atmospheric Hg^{2+} input has the smallest contribution, accounting for 3−11% (mean for branch−bark−stem: 4 ± 9, 5 ± 9, and 4 ± 9%, respectively) of Hg in woody biomass. For the underground woody biomass (small−medium−large root), atmospheric Hg^0 input accounts for 44−83% (mean for small−medium−large: 59 ± 25, 55 ± 25, and 64 ± 25%, respectively) and geological Hg input takes 12−46% (mean for small−medium−large: 33 ± 14, 32 ± 14, and 26 ± 14%, respectively). The higher Hg^0 fractions in the above ground woody biomass than in the underground woody

https://dx.doi.org/10.1021/acs.est.0c01667
Environ. Sci. Technol. 2020, 54, 8083−8093

biomass suggests a foliage-to-root transport after atmospheric uptake. The greater geological Hg and atmospheric Hg^{2+} fractions in underground woody biomass than in above ground woody biomass ($p < 0.01$, by paired t test) indicates the occurrence of geological Hg and atmospheric Hg^{2+} uptake by roots. The Hg isotopic evidence is consistent with the results from laboratory experiments that point to atmospheric Hg^0 as the dominant source in woody biomass.[37]

4.3. Hg Sources in Lichen and Moss. The ranges of Hg isotopic signatures in moss and lichen are comparable to values from earlier studies.[18,25,26,47,48] The more negative δ^{202}Hg values in the tree lichen than in the tree moss suggests that the lighter Hg isotopes in air are preferentially accumulated in the tree lichen. Photochemical Hg reduction on foliage could result in small but significant differences between foliage and atmospheric Hg^0 odd isotope MIF.[18,49,50] The more negative value of Δ^{199}Hg in the tree moss suggests a higher degree of photochemical Hg reduction. The Δ^{200}Hg values in moss and lichen grown on tree are close to 0 (average: -0.02 ± 0.04‰), indicating a small contribution from atmospheric Hg^{2+} input. Interestingly, the ground moss has more positive δ^{202}Hg, Δ^{199}Hg, and Δ^{200}Hg values than the tree moss, suggesting a greater amount of atmospheric Hg^{2+} input. The MIF mixing model confirms that atmospheric Hg^0 dominates the Hg sources in both tree and ground moss, while atmospheric Hg^{2+} contributes 24 ± 12% of Hg content in ground moss, ~2 times that of the atmospheric Hg^{2+} fraction for tree moss (Figure 4b). The higher atmospheric Hg^{2+} contribution in ground moss is likely attributed to the longer precipitation Hg residence time.

4.4. Hg Sources in Throughfall. Data of Hg isotopic signatures in throughfall remain limited in the literature. The positive Δ^{200}Hg and Δ^{199}Hg signals are mainly observed in open precipitation water in earlier studies[20,30,51,52] and in Figure 3. The Δ^{199}Hg values of PBM in remote forest sites are found to be similar to that of Hg^{2+} in precipitation water.[53] To date, only one study reported Hg MIF signatures in gaseous oxidized Hg (Δ^{199}Hg, −0.28 to +0.18‰ and Δ^{200}Hg, 0.08−0.28‰).[54] Based on these findings, the mixing of GOM, PBM, and precipitation water cannot solely explain the Hg MIF and MDF signatures in throughfall. An hypothesis is that the photoreduction of Hg^{2+} at the surface of foliage may change Hg MIF.[17,31,54] However, the much lighter ^{202}Hg in throughfall is not supported by reduction mechanisms that cause an enrichment of heavier isotopes in the residual Hg^{2+} phase.[31,55]

The measured Hg isotopic signatures in throughfall samples point to two possible sources (Figure 3a,b): precipitation Hg and atmospheric Hg^0. The Hg MIF signatures in precipitation represent the atmospheric Hg^{2+} sources, which include the rainfall Hg deposition and some dry depositions of GOM and PBM.[17,53] Using a two-endmember mixing model with MIF signatures of atmospheric Hg^0 and Hg^{2+} inputs, the contribution of atmospheric Hg^0 increases from 34 ± 19% at the 1990 retreat site to 82 ± 23% at the 1890 retreat site (Figure 4c). Surface soil dust, bark, moss covers, and other tree detritus on the canopy are possibly the important contributors since the atmospheric Hg^0 is the predominant Hg source in these samples[38] (Figure 3). The sum of Hg pool sizes in bark and moss covers on the tree is at the same level as the foliage Hg pool sizes, even 1−4 times higher at the sites of 1990−1958 retreat. Therefore, atmospheric Hg^0 uptake by these vegetation covers grown on the canopy and the subsequent mixing into precipitation contribute to a large fraction of Hg^0 sources in throughfall. Atmospheric Hg^0 directly absorbed on the surface foliage is also important contributors.[37,56]

There are two main pathways for Hg mixing into the throughfall. One is the particulate Hg derived from surface soil dust and tree detritus. However, the particle-bound Hg cannot solely contribute the sources, because its Hg concentrations in throughfall at sites of 1990−1930 retreat are comparable to values in open precipitation, except at 1890 retreat site, where the particulate Hg concentration is 5 times higher (Figure S3). The other is the aqueous Hg desorbed from surface soil dust and vegetation covers (e.g., bark, moss, foliage, etc.) on the canopy. The dissolved Hg can quickly bind to DOM (dissolved organic matter), and the elevated DOM in throughfall further enhances Hg mobility.[57−59] This is supported by the observed elevated dissolved Hg and DOM in throughfall as well as the strong correlation between them as shown in Figure S3 and earlier studies.[57,58] Few secondary processes induce Hg isotopic fractionation since Hg desorbed from soil or decomposing detritus as Hg−DOM complexes[60,61] inherit the atmospheric Hg^0 isotopic signatures. This is consistent with the trends of throughfall with higher dissolved Hg exhibiting more negative MDF and MIF signatures (Figure 3, Figure S3, and Table S3).

4.5. Enhanced Atmospheric Hg^0 Deposition by Moss/Woody Biomass and Throughfall. Our earlier work at these sites has documented the atmospheric Hg accumulation process in organic soil across the whole forest succession.[38] The Hg isotopic mixing model estimates an average of 6.1 ± 3.9 $\mu g\ m^{-2}\ yr^{-1}$ deposition flux from atmospheric Hg^{2+} sources via throughfall (Figure S4), exceeding the 4.4 $\mu g\ m^{-2}\ yr^{-1}$ atmospheric Hg^{2+} accumulation rate in the organic soils across the forest chronosequence sites.[38] This indicates that Hg^{2+} contained in throughfall is sufficient to supply atmospheric Hg^{2+} accumulated in forest soil.

The Hg deposition through litterfall has been regarded as the single largest source of Hg^0 to forest ecosystems.[11,13−15] However, the total litterfall Hg flux (leaf, twig, and some tree detritus litter) observed in this study is equivalent to 27−61% of the Hg^0 accumulation rates (Figures 4d) at sites representing a deglacial time from 1958 to 1990 and to 85% at the site of 1930 retreat. This falls short of the amount of Hg^0 accumulation in organic soil and suggests the existence of additional Hg sources from atmospheric Hg^0 deposition overlooked by earlier studies. Because the lichen cover only scatters on the limited tree stems, this study will mainly focus on the role of moss cover. Using the fluxes and pool size data, we applied the isotope mixing model to assess atmospheric Hg^0 pool (Hg^0_{PL}) and inputs (Hg^0_I) by the moss, woody biomass, and throughfall as in the following:

$$Hg^0_{PL} = THg_{PL} \times Hg^0F \quad (14)$$

$$Hg^0_I = THg_{IL} \times Hg^0F \quad (15)$$

where THg_{PL} is the total Hg pool size in moss and woody biomass, THg_{IL} is the total Hg input via throughfall, and Hg^0F is the fraction of Hg derived from the atmospheric Hg^0 sources.

Earlier studies mainly focused on moss as a bioindicator for Hg pollution levels in forest ecosystems.[27−29] Data reporting the Hg^0 pool size of moss in forest ecosystems remain scarce. The total 1.4−8.3 $\mu g\ m^{-2}$ atmospheric Hg^0 pool size (mean = 4.1 ± 3.0 $\mu g\ m^{-2}$) in live moss foliage at the sites representing

https://dx.doi.org/10.1021/acs.est.0c01667
Environ. Sci. Technol. 2020, 54, 8083−8093

glacier retreat time of 1990−1958 and 14.5 $\mu g\ m^{-2}$ pool size at the sites of 1930−1890 retreat are substantial deposition terms (Figure 4e). The atmospheric Hg^0 pool size in ground live moss foliage accounts for 34 ± 24% of total atmospheric Hg^0 pool size in live moss foliage. In addition, the atmospheric Hg^0 pool size in moss dead parts increases from 0.6 to 29.3 $\mu g\ m^{-2}$ with the forest succession of 1990−1890 retreat sites. Given the months to years of moss lifespan,[62] the Hg pool size in tree and ground moss in the whole forest chronosequence plays an important role in atmospheric Hg^0 accumulation in organic soils. This is consistent with our earlier study showing that moss biomass enhances Hg accumulation in organic soils over the glacial erratic at Mt. Gongga, Southwest China.[25]

Another pathway is by the Hg accumulation in woody biomass through foliage-to-root transport of atmospheric Hg^0 uptake and decomposition of woody biomass in forest soil. Figure 4e demonstrates that the total atmospheric Hg^0 pool size increases from 2.0 to 144.0 $\mu g\ m^{-2}$ in woody biomass at sites of 1990−1830 retreat, with an average accumulation rate of 0.9 $\mu g\ m^{-2}\ yr^{-1}$. The Hg turnover in woody biomass is slow since it takes more than 10 years for wood to decompose into organic soil.[63] Thus, the decomposition of wood biomass is less likely to contribute to the Hg accumulation in organic soils.

Mercury input via throughfall represents a significant sink of atmospheric Hg^0, which is consistent with a recent oral presentation at a Hg conference in Poland.[64] Figure 4d shows a 5−10 $\mu g\ m^{-2}\ yr^{-1}$ atmospheric Hg^0 deposition rate via the throughfall across the site of 1990−1930 retreat and up to 35.6 $\mu g\ m^{-2}\ yr^{-1}$ at the site of 1890 retreat. It is noted that the estimated annual throughfall Hg^0 flux has uncertainties because Hg isotopes in throughfall samples were collected in September−November, not the entire year. We recommend more investigation in other months in the future.

The sum of atmospheric Hg^0 deposition rate via litterfall, throughfall, and Hg^0 uptake by ground live moss (assumption of 1 year lifespan) is equivalent to 54−85% (median = 71%) of the atmospheric Hg^0 accumulation rate in organic soils across the sites of 1990−1958 retreat, to 120% at the site of 1930 retreat, and to 346% at the site of 1890 retreat. Since negative Hg^0 flux is often observed on the forest floor,[65,66] direct atmospheric Hg^0 deposition is likely an additional Hg input to the forest floor at the sites of 1990−1958 retreat. The elevated atmospheric Hg^0 deposition with decreased atmospheric Hg^0 accumulation rate at the site of 1890 retreat indicates that, as Hg accumulates, forest soil gradually turns into an atmospheric Hg^0 source likely due to the much higher soil Hg reduction at older forest succession sites. We recommend further measurements focusing on the air−soil Hg^0 exchange across the whole forest chronosequence sites to test this hypothesis.

Earlier Hg stable isotopes studies in alpine forest ecosystems showed dry deposition of Hg^0 being the primary source,[16−20] while flux data indicated atmospheric Hg^{2+} as the dominant source because of Hg deposition via precipitation and cloudwater.[13−15] Our results show that such discrepancy is most likely due to the lack of consideration in earlier flux measurements for Hg input by moss, woody biomass, and throughfall originated from atmospheric Hg^0.

4.6. Sensitivity Analysis for Hg Isotope Mixing Models. Uncertainties associated with the Hg isotopic mixing models can be divided into two categories. One is caused by the analytical precision of MIF signatures measured by MC-IMP-MS (usually 0.04‰ for one SD). These uncertainties are quantified through Monte Carlo simulations by generating one million groups of MIF signatures randomly ranging from mean − SD to mean + SD. The other is caused by the assumption of Hg isotopic signatures in each endmember. For atmospheric Hg^0 endmember, photochemical Hg reduction and re-emission on foliage could result in small but significant differences (0.10 to 0.15‰ shift, equivalent to ∼2SD level of $\Delta^{199}Hg$) between foliage versus atmospheric Hg^0 odd isotopic MIF.[50] Thus, the average MIF signatures of foliage are a better representation of atmospheric Hg^0 input endmember compared to the use of direct MIF signatures of atmospheric Hg^0. The distinct difference of $\Delta^{199}Hg$ between in foliage and in precipitation (−0.23 ± 0.05 versus 0.91 ± 0.27‰) can be qualified for distinguishing the atmospheric Hg^{2+} and Hg^0 sources; albeit, the knowledge gap in the measurement of gaseous oxidized Hg samples[67,68] renders the Hg MIF signatures of gaseous oxidized Hg uncertain.[9,60] Finally, significant $\Delta^{200}Hg$ values were mainly found in precipitation, but they were close to zero in other endmembers. This reduces the model capability in distinguishing the sources of atmospheric Hg^0 and geological Hg inputs.

The results from the two-level factorial experiments are shown and discussed in detail in Figures S5 and S6 and Section S6 of the Supporting Information. On average, an increase in Hg isotopic values of atmospheric Hg^0 endmember from mean − 2SD to mean + 2SD leads to −7 to +19% variation in estimated Hg source fractions of woody biomass and 17−21% variation of throughfall and moss covers. The atmospheric Hg^{2+} endmember influences the model results by −5 to +6% in woody biomass model estimates and by 15−18% in throughfall and moss covers model estimates. A mean − 2SD to mean + 2SD change for geological Hg endmember leads to −18 to +23% shifts in the estimated Hg source fraction in woody biomass. Increasing both the atmospheric Hg^0 and geological endmembers results in −10 to −8% significant interaction effects in the estimated geological Hg fractions. Overall, the Hg MIF values of atmospheric Hg^0 and geological endmembers are the significant factors influencing modeling results, and the uncertainties do not significantly change the results of our assessment.

5. IMPLICATIONS FOR ESTIMATING GLOBAL FOREST HG^0 SINK

Table S8 shows Hg concentrations in moss covers reported in this study and in the Arctic, Antarctic, European, and other TP regions (36−195 ng g^{-1}, mean = 98 ± 51 ng g^{-1}, n = 7120). Global carbon (C) uptake by moss covers is 3.8 Pg yr^{-1}, of which 83% is from forest ecosystems.[21] Given ∼50% of C content in moss covers[21] with 200 ± 100 ng g^{-1} Hg/C ratio, we can estimate that Hg uptake by global moss covers in forest ecosystems can reach 630 ± 315 Mg yr^{-1}. The Hg fixed in woody biomass is ∼140 Mg yr^{-1} [69] and the throughfall deposition is ∼1340 Mg yr^{-1}.[17,70] Atmospheric Hg^0 accounts for 75−90% of Hg in the moss and woody biomass and 34−82% in throughfall Hg. The three input sources (mosses, woody biomasses, and throughfall) combined contribute to a large atmospheric Hg^0 sink that increases significantly the previously estimated atmospheric Hg^0 sink via litterfall (1000−1200 Mg yr^{-1})[17,70] in global forest ecosystems. Although large uncertainties exist because of limited data availability, our findings highlight the need for future studies to better understand the role of throughfall and moss covers in the global Hg biogeochemical cycling. Such studies will enable a

https://dx.doi.org/10.1021/acs.est.0c01667
Environ. Sci. Technol. 2020, 54, 8083−8093

more accurate quantification of the global Hg^0 sink mediated through terrestrial vegetative ecosystems.

■ ASSOCIATED CONTENT

Supporting Information

The Supporting Information is available free of charge at https://pubs.acs.org/doi/10.1021/acs.est.0c01667.

Discussions of sample collection, concentration measurements, preconcentration procedure, Hg isotope measurement, and sensitivity analysis for Hg isotope mixing models, tables of Hg isotopic compositions and concentrations, contribution of atmospheric Hg^0 sources, precipitation/throughfall annual amount, leaf litter biomass production, specific fractions of Hg pool size in each plant component, biomass of each component in tree species, and average Hg concentration, and figures of Hg concentrations, DOC concentrations, atmospheric Hg^{2+} mass flow via precipitation and throughfall, atmospheric Hg^{2+} re-emission on the canopy, atmospheric Hg^{2+} accumulation rate in organic soils, and sensitivity analysis (PDF)

■ AUTHOR INFORMATION

Corresponding Authors

Xun Wang − *Interdisciplinary Research Centre for Agriculture Green Development in Yangtze River Basin, College of Resources and Environment, Southwest University, Chongqing 400715, China; State Key Laboratory of Environmental Geochemistry, Institute of Geochemistry, Chinese Academy of Sciences, Guiyang 550081, China;* orcid.org/0000-0002-7407-8965; Phone: +8617785003956; Email: wangxun@swu.edu.cn

Xinbin Feng − *State Key Laboratory of Environmental Geochemistry, Institute of Geochemistry, Chinese Academy of Sciences, Guiyang 550081, China; Center for Excellence in Quaternary Science and Global Change, Chinese Academy of Sciences, Xian 710061, China;* orcid.org/0000-0002-7462-8998; Phone: +86-851-5895728; Email: fengxinbin@vip.skleg.cn

Authors

Wei Yuan − *State Key Laboratory of Environmental Geochemistry, Institute of Geochemistry, Chinese Academy of Sciences, Guiyang 550081, China*

Che-Jen Lin − *Center for Advances in Water and Air Quality and Department of Civil and Environmental Engineering, Lamar University, Beaumont, Texas 77710, United States*

Ji Luo − *Key Laboratory of Mountain Surface Processes and Ecological Regulation, Institute of Mountain Hazards and Environment, Chinese Academy of Sciences & Ministry of Water Conservancy, Chengdu 610041, China*

Feiyue Wang − *Centre for Earth Observation Science, and Department of Environment and Geography, University of Manitoba, Winnipeg, Manitoba R3T 2N2, Canada;* orcid.org/0000-0001-5297-0859

Xuewu Fu − *State Key Laboratory of Environmental Geochemistry, Institute of Geochemistry, Chinese Academy of Sciences, Guiyang 550081, China; Center for Excellence in Quaternary Science and Global Change, Chinese Academy of Sciences, Xian 710061, China;* orcid.org/0000-0002-5174-7150

Chen Liu − *State Key Laboratory of Environmental Geochemistry, Institute of Geochemistry, Chinese Academy of Sciences, Guiyang 550081, China*

Complete contact information is available at: https://pubs.acs.org/10.1021/acs.est.0c01667

Notes

The authors declare no competing financial interest.

■ ACKNOWLEDGMENTS

This work was funded by the Strategic Priority Research Programs of the Chinese Academy of Sciences, the Pan-Third Pole Environment Study for a Green Silk Road (Pan-TPE, XDA2004050201), the National Natural Science Foundation of China (41977272), Fundamental Research Funds for the Central Universities (SWU019037), and the National Natural Science Foundation of China (41703135, 41829701, 41430754 and 41771062).

■ REFERENCES

(1) Beal, S. A.; Osterberg, E. C.; Zdanowicz, C. M.; Fisher, D. A. Ice Core Perspective on Mercury Pollution during the Past 600 Years. *Environ. Sci. Technol.* **2015**, *49* (13), 7641−7647.

(2) Eyrikh, S.; Eichler, A.; Tobler, L.; Malygina, N.; Papina, T.; Schwikowski, M. A 320 Year Ice-Core Record of Atmospheric Hg Pollution in the Altai, Central Asia. *Environ. Sci. Technol.* **2017**, *51* (20), 11597−11606.

(3) Kang, S. C.; Huang, J.; Wang, F. Y.; Zhang, Q. G.; Zhang, Y. L.; Li, C. L.; Wang, L.; Chen, P. F.; Sharma, C. M.; Li, Q.; Sillanpaa, M.; Hou, J. Z.; Xu, B. Q.; Guo, J. M. Atmospheric Mercury Depositional Chronology Reconstructed from Lake Sediments and Ice Core in the Himalayas and Tibetan Plateau. *Environ. Sci. Technol.* **2016**, *50* (6), 2859−2869.

(4) Schuster, P. F.; Krabbenhoft, D. P.; Naftz, D. L.; Cecil, L. D.; Olson, M. L.; Dewild, J. F.; Susong, D. D.; Green, J. R. A 270-year ice core record of atmospheric mercury deposition to western North America. *Geochim. Cosmochim. Acta, Suppl.* **2001**, *69* (10), A208.

(5) Enrico, M.; Le Roux, G.; Heimburger, L. E.; Van Beek, P.; Souhaut, M.; Chmeleff, J.; Sonke, J. E. Holocene Atmospheric Mercury Levels Reconstructed from Peat Bog Mercury Stable Isotopes. *Environ. Sci. Technol.* **2017**, *51* (11), 5899−5906.

(6) Pokharel, A. K.; Obrist, D. Fate of mercury in tree litter during decomposition. *Biogeosciences* **2011**, *8* (9), 2507−2521.

(7) Lindberg, S.; Bullock, R.; Ebinghaus, R.; Engstrom, D.; Feng, X. B.; Fitzgerald, W.; Pirrone, N.; Prestbo, E.; Seigneur, C. A synthesis of progress and uncertainties in attributing the sources of mercury in deposition. *Ambio* **2007**, *36* (1), 19−32.

(8) Zhang, L. M.; Wu, Z. Y.; Cheng, I.; Wright, L. P.; Olson, M. L.; Gay, D. A.; Risch, M. R.; Brooks, S.; Castro, M. S.; Conley, G. D.; Edgerton, E. S.; Holsen, T. M.; Luke, W.; Tordon, R.; Weiss-Penzias, P. The Estimated Six-Year Mercury Dry Deposition Across North America. *Environ. Sci. Technol.* **2016**, *50* (23), 12864−12873.

(9) Wright, L. P.; Zhang, L.; Marsik, F. J. Overview of mercury dry deposition, litterfall, and throughfall studies. *Atmos. Chem. Phys.* **2016**, *16* (21), 13399−13416.

(10) Wang, X.; Bao, Z.; Lin, C.-J.; Yuan, W.; Feng, X. Assessment of Global Mercury Deposition through Litterfall. *Environ. Sci. Technol.* **2016**, *50* (16), 8548−8557.

(11) Obrist, D.; Kirk, J. L.; Zhang, L.; Sunderland, E. M.; Jiskra, M.; Selin, N. E. A review of global environmental mercury processes in response to human and natural perturbations: Changes of emissions, climate, and land use. *Ambio* **2018**, *47* (2), 116−140.

(12) Kwon, S. Y.; Blum, J. D.; Yin, R.; Tsui, M. T.-K.; Yang, Y. H.; Choi, J. W. Mercury stable isotopes for monitoring the effectiveness of the Minamata Convention on Mercury. *Earth-Sci. Rev.* **2020**, *203*, 103111.

(13) Blackwell, B. D.; Driscoll, C. T. Using foliar and forest floor mercury concentrations to assess spatial patterns of mercury deposition. *Environ. Pollut.* **2015**, *202*, 126−134.
(14) Gerson, J. R.; Driscoll, C. T.; Demers, J. D.; Sauer, A. K.; Blackwell, B. D.; Montesdeoca, M. R.; Shanley, J. B.; Ross, D. S. Deposition of mercury in forests across a montane elevation gradient: Elevational and seasonal patterns in methylmercury inputs and production. *J. Geophys. Res.: Biogeosci.* **2017**, *122* (8), 1922−1939.
(15) Townsend, J. M.; Driscoll, C. T.; Rimmer, C. C.; McFarland, K. P. Avian, Salamander, and Forest Floor Mercury Concentrations Increase with Elevation in a Terrestrial Ecosystem. *Environ. Toxicol. Chem.* **2014**, *33* (1), 208−215.
(16) Wang, X.; Luo, J.; Yin, R.; Yuan, W.; Lin, C.-J.; Sommar, J.; Feng, X.; Wang, H.; Lin, C. Using Mercury Isotopes To Understand Mercury Accumulation in the Montane Forest Floor of the Eastern Tibetan Plateau. *Environ. Sci. Technol.* **2017**, *51* (2), 801−809.
(17) Zheng, W.; Obrist, D.; Weis, D.; Bergquist, B. A. Mercury isotope compositions across North American forests. *Global Biogeochem Cy* **2016**, *30* (10), 1475−1492.
(18) Enrico, M.; Le Roux, G.; Marusczak, N.; Heimburger, L. E.; Claustres, A.; Fu, X. W.; Sun, R. Y.; Sonke, J. E. Atmospheric Mercury Transfer to Peat Bogs Dominated by Gaseous Elemental Mercury Dry Deposition. *Environ. Sci. Technol.* **2016**, *50* (5), 2405−2412.
(19) Jiskra, M.; Wiederhold, J. G.; Skyllberg, U.; Kronberg, R.-M.; Hajdas, I.; Kretzschmar, R. Mercury Deposition and Re-emission Pathways in Boreal Forest Soils Investigated with Hg Isotope Signatures. *Environ. Sci. Technol.* **2015**, *49* (12), 7188−7196.
(20) Demers, J. D.; Blum, J. D.; Zak, D. R. Mercury isotopes in a forested ecosystem: Implications for air-surface exchange dynamics and the global mercury cycle. *Global Biogeochem Cy* **2013**, *27* (1), 222−238.
(21) Elbert, W.; Weber, B.; Burrows, S.; Steinkamp, J.; Buedel, B.; Andreae, M. O.; Poeschl, U. Contribution of cryptogamic covers to the global cycles of carbon and nitrogen. *Nat. Geosci.* **2012**, *5* (7), 459−462.
(22) Bargagli, R. Atmospheric chemistry of mercury in Antarctica and the role of cryptogams to assess deposition patterns in coastal ice-free areas. *Chemosphere* **2016**, *163*, 202−208.
(23) Klos, A.; Rajfur, M.; Sramek, I.; Waclawek, M. Mercury concentration in lichen, moss and soil samples collected from the forest areas of Praded and Glacensis Euroregions (Poland and Czech Republic). *Environ. Monit. Assess.* **2012**, *184* (11), 6765−6774.
(24) Shao, J. J.; Liu, C. B.; Zhang, Q. H.; Fu, J. J.; Yang, R. Q.; Shi, J. B.; Cai, Y.; Jiang, G. B. Characterization and speciation of mercury in mosses and lichens from the high-altitude Tibetan Plateau. *Environ. Geochem. Health* **2017**, *39* (3), 475−482.
(25) Wang, X.; Yuan, W.; Feng, X.; Wang, D.; Luo, J. Moss facilitating mercury, lead and cadmium enhanced accumulation in organic soils over glacial erratic at Mt. Gongga, China. *Environ. Pollut.* **2019**, *254*, 112974.
(26) Olson, C. L.; Jiskra, M.; Sonke, J. E.; Obrist, D. Mercury in tundra vegetation of Alaska: Spatial and temporal dynamics and stable isotope patterns. *Sci. Total Environ.* **2019**, *660*, 1502−1512.
(27) Bargagli, R. Moss and lichen biomonitoring of atmospheric mercury: A review. *Sci. Total Environ.* **2016**, *572*, 216−231.
(28) Bargagli, R.; Monaci, F.; Bucci, C. Environmental biogeochemistry of mercury in Antarctic ecosystems. *Soil Biol. Biochem.* **2007**, *39* (1), 352−360.
(29) Harmens, H.; Norris, D. A.; Koerber, G. R.; Buse, A.; Steinnes, E.; Ruehling, A. Temporal trends (1990−2000) in the concentration of cadmium, lead and mercury in mosses across Europe. *Environ. Pollut.* **2008**, *151* (2), 368−376.
(30) Chen, J. B.; Hintelmann, H.; Feng, X. B.; Dimock, B. Unusual fractionation of both odd and even mercury isotopes in precipitation from Peterborough, ON. *Geochim. Cosmochim. Acta* **2012**, *90*, 33−46.
(31) Blum, J. D.; Sherman, L. S.; Johnson, M. W. Mercury Isotopes in Earth and Environmental Sciences. *Annu. Rev. Earth Planet. Sci.* **2014**, *42*, 249−269.
(32) Rea, A. W.; Keeler, G. J.; Scherbatskoy, T. The deposition of mercury in throughfall and litterfall in the lake champlain watershed: A short-term study. *Atmos. Environ.* **1996**, *30* (19), 3257−3263.
(33) Rea, A. W.; Lindberg, S. E.; Keeler, G. J. Dry deposition and foliar leaching of mercury and selected trace elements in deciduous forest throughfall. *Atmos. Environ.* **2001**, *35* (20), 3453−3462.
(34) Grigal, D. F. Mercury sequestration in forests and peatlands: A review. *J. Environ. Qual.* **2003**, *32* (2), 393−405.
(35) Wang, X.; Yuan, W.; Lu, Z. Y.; Lin, C. J.; Yin, R. S.; Li, F.; Feng, X. B. Effects of Precipitation on Mercury Accumulation on Subtropical Montane Forest Floor: Implications on Climate Forcing. *J. Geophys. Res.: Biogeosci.* **2019**, *124* (4), 959−972.
(36) Yang, Y.; Yanai, R. D.; Montesdeoca, M.; Driscoll, C. T. Measuring mercury in wood: challenging but important. *Int. J. Environ. Anal. Chem.* **2017**, *97* (5), 456−467.
(37) Arnold, J.; Gustin, M. S.; Weisberg, P. J. Evidence for Nonstomatal Uptake of Hg by Aspen and Translocation of Hg from Foliage to Tree Rings in Austrian Pine. *Environ. Sci. Technol.* **2018**, *52* (3), 1174−1182.
(38) Wang, X.; Luo, J.; Yuan, W.; Lin, C. J.; Wang, F.; Liu, C.; Wang, G.; Feng, X. Global warming accelerates uptake of atmospheric mercury in regions experiencing glacier retreat. *Proc. Natl. Acad. Sci. U. S. A.* **2020**, *117* (4), 2049−2055.
(39) Wang, X.; Luo, J.; Lin, C.-J.; Wang, D.; Yuan, W. Elevated cadmium pollution since 1890s recorded by forest chronosequence in deglaciated region of Gongga. *Environ. Pollut.* **2020**, *260*, 114082.
(40) Wang, X.; Lin, C. J.; Lu, Z. Y.; Zhang, H.; Zhang, Y. P.; Feng, X. B. Enhanced accumulation and storage of mercury on subtropical evergreen forest floor: Implications on mercury budget in global forest ecosystems. *J. Geophys. Res.: Biogeosci.* **2016**, *121* (8), 2096−2109.
(41) United States Environmental Protection Agency. Method 1631, Revision B: Mercury in Water by Oxidation, Purge and Trap, and Cold Vapor Atomic Fluorescence Spectrometry. *National Service Center for Environmental Publications (NSCEP)* 1999, 1−33.
(42) Li, K.; Lin, C.-J.; Yuan, W.; Sun, G.; Fu, X.; Feng, X. An improved method for recovering and preconcentrating mercury in natural water samples for stable isotope analysis. *J. Anal. At. Spectrom.* **2019**, *34* (11), 2303−2313.
(43) Blum, J. D.; Bergquist, B. A. Reporting of variations in the natural isotopic composition of mercury. *Anal. Bioanal. Chem.* **2007**, *388* (2), 353−359.
(44) Estrade, N.; Carignan, J.; Sonke, J. E.; Donard, O. F. X. Measuring Hg Isotopes in Bio-Geo-Environmental Reference Materials. *Geostand. Geoanal. Res.* **2010**, *34* (1), 79−93.
(45) Yang, D.; Luo, J.; She, J.; Tang, R. Dynamics of Vegetation Biomass Along the Chronosequence in Hailuogou Glacier Retreated Area, Mt. Gongga. *Ecology and Environmental Sciences* **2015**, *24* (11), 1843−1850.
(46) Scanlon, T. M.; Riscassi, A. L.; Demers, J. D.; Camper, T. D.; Lee, T. R.; Druckenbrod, D. L. Mercury Accumulation in Tree Rings: Observed Trends in Quantity and Isotopic Composition in Shenandoah National Park, Virginia. *J. Geophys. Res.: Biogeosci.* **2020**, *125* (2), 1.
(47) Sonke, J. E. A global model of mass independent mercury stable isotope fractionation. *Geochim. Cosmochim. Acta* **2011**, *75* (16), 4577−4590.
(48) Ma, J.; Hintelmann, H.; Kirk, J.; Muir, D. Mercury and its isotope composition in lichens and sediments from particular pollution source. *Geochim. Cosmochim. Acta, Suppl.* **2010**, *74* (12), A649.
(49) Yu, B.; Fu, X.; Yin, R.; Zhang, H.; Wang, X.; Lin, C.-J.; Wu, C.; Zhang, Y.; He, N.; Fu, P.; Wang, Z.; Shang, L.; Sommar, J.; Sonke, J. E.; Maurice, L.; Guinot, B.; Feng, X. Isotopic Composition of Atmospheric Mercury in China: New Evidence for Sources and Transformation Processes in Air and in Vegetation. *Environ. Sci. Technol.* **2016**, *50* (17), 9262−9.
(50) Yuan, W.; Sommar, J.; Lin, C.-J.; Wang, X.; Li, K.; Liu, Y.; Zhang, H.; Lu, Z.; Wu, C.; Feng, X. Stable Isotope Evidence Shows

https://dx.doi.org/10.1021/acs.est.0c01667
Environ. Sci. Technol. 2020, 54, 8083−8093

Re-emission of Elemental Mercury Vapor Occurring after Reductive Loss from Foliage. *Environ. Sci. Technol.* **2019**, *53* (2), 651−660.
(51) Wang, Z. H.; Chen, J. B.; Feng, X. B.; Hintelmann, H.; Yuan, S. L.; Cai, H. M.; Huang, Q.; Wang, S. X.; Wang, F. Y. Mass-dependent and mass-independent fractionation of mercury isotopes in precipitation from Guiyang, SW China. *C. R. Geosci.* **2015**, *347* (7−8), 358−367.
(52) Yuan, S.; Zhang, Y.; Chen, J.; Kang, S.; Zhang, J.; Feng, X.; Cai, H.; Wang, Z.; Wang, Z.; Huang, Q. Large Variation of Mercury Isotope Composition During a Single Precipitation Event at Lhasa City, Tibetan Plateau. *Procedia Earth Planet. Sci.* **2015**, *13*, 282−286.
(53) Fu, X.; Zhang, H.; Feng, X.; Tan, Q.; Ming, L.; Liu, C.; Zhang, L. Domestic and Transboundary Sources of Atmospheric Particulate Bound Mercury in Remote Areas of China: Evidence from Mercury Isotopes. *Environ. Sci. Technol.* **2019**, *53* (4), 1947−1957.
(54) Rolison, J. M.; Landing, W. M.; Luke, W.; Cohen, M.; Salters, V. J. M. Isotopic composition of species-specific atmospheric Hg in a coastal environment. *Chem. Geol.* **2013**, *336*, 37−49.
(55) Sonke, J. E.; Blum, J. D. Advances in mercury stable isotope biogeochemistry Preface. *Chem. Geol.* **2013**, *336*, 1−4.
(56) Stamenkovic, J.; Gustin, M. S. Nonstomatal versus Stomatal Uptake of Atmospheric Mercury. *Environ. Sci. Technol.* **2009**, *43* (5), 1367−1372.
(57) Akerblom, S.; Meili, M.; Bishop, K. Organic Matter in Rain: An Overlooked Influence on Mercury Deposition. *Environ. Sci. Technol. Lett.* **2015**, *2* (4), 128−132.
(58) Hojdova, M.; Huang, J. H.; Kalbitz, K.; Matzner, E. Effects of throughfall and litterfall manipulation on concentrations of methylmercury and mercury in forest-floor percolates. *J. Plant Nutr. Soil Sci.* **2007**, *170* (3), 373−377.
(59) Kolka, R. K.; Grigal, D. F.; Nater, E. A.; Verry, E. S. Hydrologic cycling of mercury and organic carbon in a forested upland-bog watershed. *Soil Sci. Soc. Am. J.* **2001**, *65* (3), 897−905.
(60) Jiskra, M.; Wiederhold, J. G.; Skyllberg, U.; Kronberg, R. M.; Kretzschmar, R. Source tracing of natural organic matter bound mercury in boreal forest runoff with mercury stable isotopes. *Environmental Science Processes & Impacts* **2017**, *19* (10), 1235.
(61) Woerndle, G. E.; Tsui, M. T.-K.; Sebestyen, S. D.; Blum, J. D.; Nie, X.; Kolka, R. K. New Insights on Ecosystem Mercury Cycling Revealed by Stable Isotopes of Mercury in Water Flowing from a Headwater Peatland Catchment. *Environ. Sci. Technol.* **2018**, *52* (4), 1854−1861.
(62) Puglisi, M.; Minissale, P.; Sciandrello, S.; Privitera, M. Life syndrome of the bryophyte communities as an adaptative pattern in the Mediterranean temporary ponds of Italy. *Plant Biosyst.* **2016**, *150* (6), 1417−1425.
(63) Bradford, M. A.; Warren, R. J., II; Baldrian, P.; Crowther, T. W.; Maynard, D. S.; Oldfield, E. E.; Wieder, W. R.; Wood, S. A.; King, J. R. Climate fails to predict wood decomposition at regional scales. *Nat. Clim. Change* **2014**, *4* (7), 625−630.
(64) Li, K. Identification of Mercury Souces in Throughfall Using Stable Isotope Signatures. *14th International Conference on Mercury as a Global Pollutant: ICMGP 2019*, Krakow, Poland, Sept 8−13, 2019.
(65) Zhu, W.; Lin, C. J.; Wang, X.; Sommar, J.; Fu, X.; Feng, X. Global observations and modeling of atmosphere−surface exchange of elemental mercury: a critical review. *Atmos. Chem. Phys.* **2016**, *16* (7), 4451−4480.
(66) Agnan, Y.; Le Dantec, T.; Moore, C. W.; Edwards, G. C.; Obrist, D. New Constraints on Terrestrial Surface Atmosphere Fluxes of Gaseous Elemental Mercury Using a Global Database. *Environ. Sci. Technol.* **2016**, *50* (2), 507−524.
(67) Gustin, M. S.; Amos, H. M.; Huang, J.; Miller, M. B.; Heidecorn, K. Measuring and modeling mercury in the atmosphere: a critical review. *Atmos. Chem. Phys.* **2015**, *15* (10), 5697−5713.
(68) Huang, J. Y.; Gustin, M. S. Uncertainties of Gaseous Oxidized Mercury Measurements Using KCl-Coated Denuders, Cation-Exchange Membranes, and Nylon Membranes: Humidity Influences. *Environ. Sci. Technol.* **2015**, *49* (10), 6102−6108.
(69) Obrist, D. Atmospheric mercury pollution due to losses of terrestrial carbon pools? *Biogeochemistry* **2007**, *85* (2), 119−123.
(70) Fu, X.; Zhu, W.; Zhang, H.; Sommar, J.; Yu, B.; Yang, X.; Wang, X.; Lin, C.-J.; Feng, X. Depletion of atmospheric gaseous elemental mercury by plant uptake at Mt. Changbai, Northeast China. *Atmos. Chem. Phys.* **2016**, *16* (20), 12861−12873.

https://dx.doi.org/10.1021/acs.est.0c01667
Environ. Sci. Technol. 2020, 54, 8083−8093